Four-dimensional point spread functions—A powerful tool to reconstruct the source image in neutron coded imaging

Article *in* Nuclear Instruments and Methods in Physics Research Section A Accelerators Spectrometers Detectors and Associated Equipment · June 2022

DOI: 10.1016/j.nima.2022.167038

CITATIONS
0

READS
33

5 authors, including:

Huasi Hu
Xi'an Jiaotong University
65 PUBLICATIONS **318** CITATIONS

SEE PROFILE

Guang Hu
Xi'an Jiaotong University
34 PUBLICATIONS **124** CITATIONS

SEE PROFILE

Nuclear Inst. and Methods in Physics Research, A 1039 (2022) 167038

Contents lists available at ScienceDirect

Nuclear Inst. and Methods in Physics Research, A

journal homepage: www.elsevier.com/locate/nima

Four-dimensional point spread functions—A powerful tool to reconstruct the source image in neutron coded imaging

Mingfei Yan [a,b,*], Huasi Hu [a,*], Guang Hu [a], Yihong Yan [a], Zhihua Liu [c]

[a] School of Energy and Power Engineering, Xi'an Jiaotong University, Xi'an 710049, China
[b] RIKEN Center for Advanced Photonics, RIKEN, Wako Saitama 351-0198, Japan
[c] Department of Nuclear, Plasma and Radiological Engineering, University of Illinois at Urbana-Champaign, Champaign 61820, USA

ARTICLE INFO

Keywords:
Neutron coded imaging
Coded apertures
MCNP6
Point spread function
Spatially translational variance
System alignment
Image reconstruction

ABSTRACT

Neutron coded imaging has been developed as a powerful tool to diagnose the two-dimensional (2-D) shape and size of a deuterium–tritium (DT) plasma in nuclear fusion. Compared with direct neutron radiography, it can extend the spatial resolution of the imaging system, whereas the image reconstruction process is necessary to deblur the coded image due to existence of the coded aperture. The Current reconstruction scheme is based on the linear imaging system, which requires the point spread function (PSF) at the center of field of view (FOV). However, there are three limitations with respect to imaging quality under this reconstruction scheme: one is the destruction of linear system as the coded aperture size increasing; one is the spatially translational variance of point spread function (PSF); another one is the system misalignment. Therefore, the coded aperture needs to be well designed to address those limitations. In this paper, we proposed a novel reconstruction scheme for neutron coded imaging with four-dimensional (4D) PSFs. Systematical comparisons of reconstructions with PSF at the center of FOV and 4D PSFs within FOV were performed. The results show reconstructions with 4D PSFs always achieve a similar accuracy no matter with the type and size of coded apertures, as well as precision of system alignment, whereas those with the PSF at the center of FOV show a different but lower accuracy. 4D PSFs are recommended to reconstruct the source image in neutron coded imaging.

1. Introduction

Neutron coded imaging [1–4] has been developed as an important tool to diagnose the thermonuclear ignition of a deuterium–tritium (D–T) plasma. It is used to measure the size, shape and symmetry of D–T reaction by employing 14.1 MeV fast neutron emitted from the fusion reaction zone. Those parameters can be used to predict the success of reaching ignition and regarded as the reference for capsule design. As shown in Fig. 1, the neutron coded imaging system is composed of a fusion neutron source, a coded aperture made of high-Z material, such as gold and tungsten, and a scintillator-based imaging detector. The magnification system is formed with the coded aperture, where the magnification coefficient is a ratio of L_2 to L_1. Hence, the spatial resolution of the system, limited by the detector, is greatly extended [5]. Although higher spatial resolution is offered, blurred image, termed as coded image, is formed due to existence of the coded aperture. The reconstruction process is necessary to obtain high quality image. The current reconstruction scheme is based on the linear imaging system, which requires the point spread function (PSF) at the center of field of view (FOV), where PSF is defined as the detector response with respect to a point source [6,7]. Under the scheme, unfolding algorithms [8,9] with convolution theorem, developed in optical or X (γ)-ray fields, were widely applied to reconstruct the source image in neutron coded imaging. However, there are three limitations with respect to imaging quality under this scheme: one is the destruction of linear system as the coded aperture size increasing; one is the spatially translational variance of PSF; another one is the system misalignment.

At the early years of fusion diagnosis, pin hole [10,11], widely used in optical imaging, was applied in neutron coded imaging due to its high spatial resolution. Besides the spatial resolution, signal to noise ratio (SNR) is another crucial factor in terms of imaging quality. To achieve a high SNR image, a larger-size aperture is expected. Cone hole [12,13] and array hole [14,15] were designed under this requirement. However, larger-size aperture may lead to lower spatial resolution, while destruction of the linear characteristic of imaging system. Thus a compromise between resolution and SNR needs to be weighted in coded aperture design.

Because 14.1 MeV fast neutron has a mean free pass of 3 cm in gold and tungsten, the coded aperture does not behave as it in optical or X (γ)-ray coded imaging. Its edge can be transmitted by the fast neutron, which makes the PSF spatially translational variance to some

* Corresponding authors.
E-mail addresses: ffww123@stu.xjtu.edu.cn, mingfei.yan@riken.jp (M. Yan), huasi_hu@mail.xjtu.edu.cn (H. Hu).

https://doi.org/10.1016/j.nima.2022.167038
Received 1 February 2022; Received in revised form 14 May 2022; Accepted 31 May 2022
Available online 26 June 2022
0168-9002/

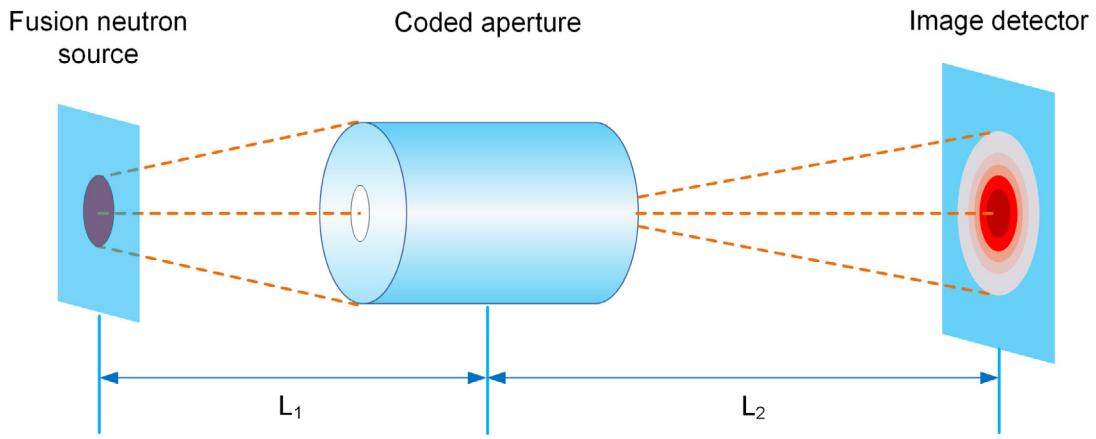

Fig. 1. Neutron coded imaging.

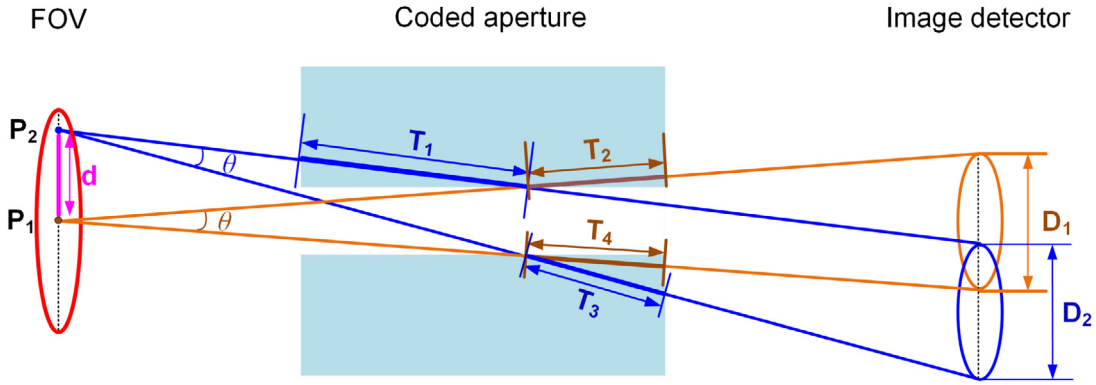

Fig. 2. Source of spatially translational variance PSF.

extent. As shown in Fig. 2, the intercepts between the neutron paths and the coded aperture are different, i.e. $T_1 \neq T_2$ and $T_3 \neq T_4$, in case of the point source located at or off the center of FOV, respectively, leading to the difference in D_1 and D_2. Image reconstruction under the current scheme, which only employs the PSF at the center of FOV, may result in poor imaging quality. The problem is more severe in diagnosing large size neutron source as Z-pinch driven fusion source (~cm) [16]. Although the problem could be partially solved by developing a spatially translational invariance coded aperture [17,18], the design of a coded aperture with high resolution and SNR, along with spatially translational invariance, is a challenge. Moreover, the current scheme also requires well alignment of the source center, coded aperture center and detector center [19]. It indicates the necessity of establishing an alignment system for neutron coded imaging.

To address the limitations above, we proposed a novel reconstruction scheme for neutron coded imaging with four-dimensional (4D) PSFs. The performances of the two types of reconstruction schemes were comparatively studied. The contents of this paper were organized as follows: firstly, the mathematical theory of coded image reconstruction was introduced; secondly, the PSFs of Z-pinch neutron source imaging system were simulated by the Monte Carlo code MCNP6, and the spatially translational invariance of different types of coded apertures was quantitatively compared; thirdly, the systematical comparisons of reconstructions with PSF at the center of FOV and with 4D PSFs for different complexities of phantoms under different types of apertures were performed in case of the source at and off the center of FOV, respectively.

2. Materials and methods

2.1. Theory of coded image reconstruction

The code image reconstruction shares the common image reconstruction theory. It can be described as a constraint optimization problem. In consideration of the sparse characteristic of image gradient [20], the objective function is either:

$$\hat{\boldsymbol{X}} = \arg\min_{\boldsymbol{X}\geq\boldsymbol{0}} \|\boldsymbol{Y} - \boldsymbol{P} \otimes \boldsymbol{X}\|_2^2 + \alpha_{\mathrm{TV}} \cdot \iint \|\nabla \boldsymbol{X}\|_2 \, dxdy \tag{1}$$

or:

$$\hat{\boldsymbol{X}} = \arg\min_{\boldsymbol{X}\geq\boldsymbol{0}} \|\boldsymbol{Y} - \boldsymbol{M} \cdot \boldsymbol{X}\|_2^2 + \alpha_{\mathrm{TV}} \cdot \iint \|\nabla \boldsymbol{X}\|_2 \, dxdy \tag{2}$$

Where $\boldsymbol{Y} = \left(y_1, y_2, \cdots, y_{\mathrm{i}}, \cdots, y_{\mathrm{R}}\right)^{\mathrm{T}}$, $\boldsymbol{P} = \left(p_{\mathrm{ij}}\right) \in \boldsymbol{P}^{\mathrm{R}} \times \boldsymbol{P}^{\mathrm{S}}$, $\boldsymbol{M} = \left(m_{\mathrm{ij}}\right) \in \boldsymbol{M}^{\mathrm{R}} \times \boldsymbol{M}^{\mathrm{S}}$, and $\boldsymbol{X} = \left(x_1, x_2, \cdots, x_{\mathrm{j}}, \cdots, x_{\mathrm{S}}\right)^{\mathrm{T}}$ are termed as coded image, PSF at the center of FOV, 4D PSFs within FOV and source image to be reconstructed, respectively; $\otimes$ represents two-dimensional (2D) convolution; $\cdot$ represents multiplication; $\iint \|\nabla \boldsymbol{X}\|_2 \, dxdy$ and α_{TV} are the sparse constraint term and sparse coefficient, respectively. Coded image represents the detector response to the source to be diagnosed, which is obtained from real measurement or theoretical calculation. Fig. 3 shows two types of PSF used in neutron coded imaging. PSF at the center of FOV is calculated by assuming a point source located at the center of the source plane; 4D PSFs within FOV are obtained from PSFs calculated by assuming a point source located at each position of the source plane, respectively. The differences between the two equations are that only PSF at the center of FOV is utilized in Eq. (1), while 4D PSFs at different positions within FOV are utilized in Eq. (2).

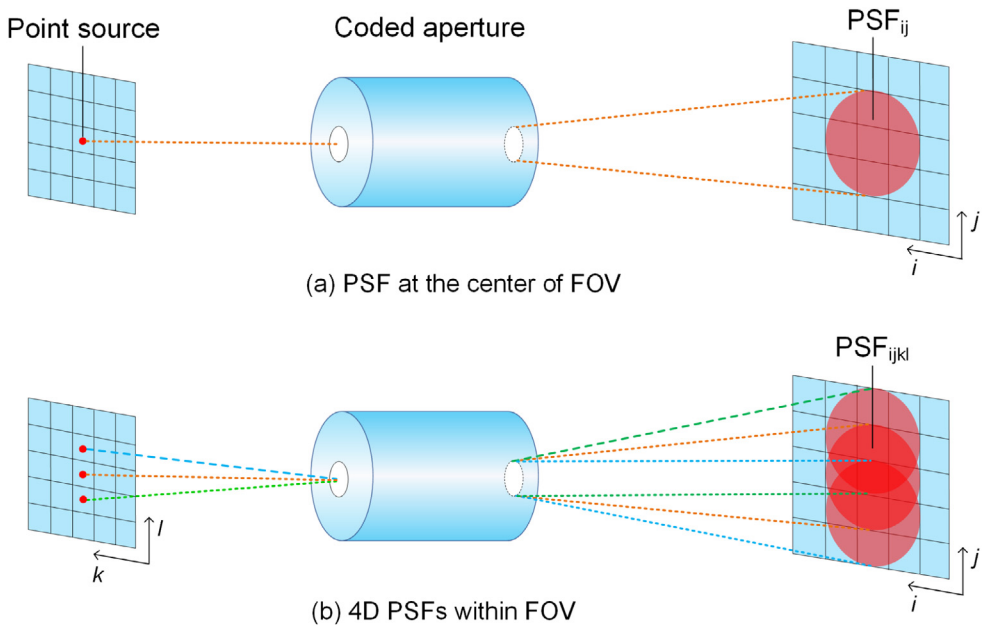

Fig. 3. Two types of PSF used in neuron coded imaging.

To ensure the comparisons of reconstructions with PSF at the center of FOV and with 4D PSFs under a fair environment, the same algorithm to solve Eqs. (1) and (2) is necessary. In our previous study, a heuristic algorithm, an improved adaptive genetic algorithm (IAGA) [7], was proposed to solve the equations adequately, albeit no other algorithms reported. The algorithm executed as: the pixel value on an initial image was randomly assigned; then the image evolved through selection, crossover, and mutation operations until the residual met the convergence condition; finally the reconstructed image was obtained. IAGA was proved to be a better algorithm with respect to the reconstruction accuracy than other commonly used deterministic algorithms to solve inverse problems. Therefore, it was applied to the image reconstruction in this paper.

2.2. Monte Carlo simulation

Fig. 4 shows the neutron coded imaging setup for diagnosis of Z-pinch driven fusion source that emits 14.1 MeV neutrons. The detector is scintillation fiber arrays, consisting of 199 × 199 pixels with a size of 500 μm×500 μm×5 cm (thickness). The magnification of whole system is 5. Different types of aperture curves were applied in this study: pin hole, cone hole, array hole and inverse radius of curvature (IRC) hole. Specifications of each aperture are shown in Fig. 5: pin hole has a diameter of 0.5 cm; cone hole is made of two stages with the left-to-right diameters of 0.5 cm, 0.6 cm and 1.2 cm, respectively; array hole consists of 6 pin holes, among which the central one has a diameter of 0.2 cm, and the 5 surrounded ones have 0.25 cm in diameter; the radius of curvature of IRC hole varies inversely with distance from the source plane, with the left-to-right diameters of 0.5 cm, 0.48 cm and 0.6 cm, respectively. In this study, PSFs and coded images were simulated by the Monte Carlo code MCNP6 [21] with ENDF/B-VII.1 cross section library, where the energy deposition of recoil protons, from the elastic scattering reaction of neutron and hydrogen in the fiber core, is tallied as detector responses. In PSFs simulation, 0.98×0.98 cm^2 fusion source is divided into 99 × 99 meshes, the center of which is placed with a point source one by one. The neutron yield of the fusion source is assumed to be 10^{12} n/s.

PSFs for different types of coded apertures are shown in Fig. 6, where at the first row are simulated PSFs with source at the center of FOV; at the second row are simulated PSFs with source off the center of FOV by 0.49 cm horizontally and 0.49 cm vertically; at the third row are PSFs obtained by translation of the PSF with source at the center of FOV, with the left pixels filled with 0. PSFs at the first row indicate that the neutron intensities at central area are high and the edge areas are blurred; they are rotationally symmetric for pin hole, cone hole, and IRC hole because their centers are the same as the center of FOV, except for the 5 surrounded ones in array hole because they are off the center of FOV. It can be understood as spatially translational variance of PSF. It is more evident as the off-center distance increases, as shown in figures at the second row. The degree of spatially translational variance of PSFs can be quantitatively measured by correlation coefficient (CC):

$$cc = \frac{\sum_{\mathrm{j}=1}^{\mathrm{Q}} \left(f_{sim.}^{(\mathrm{j})} - \overline{f}_{sim.}^{(\mathrm{j})}\right)\left(f_{tran.}^{(\mathrm{j})} - \overline{f}_{tran.}^{(\mathrm{j})}\right)}{\sqrt{\sum_{\mathrm{j}=1}^{\mathrm{Q}} \left(f_{\mathrm{sim.}}^{(\mathrm{j})} - \overline{f}_{sim.}^{(\mathrm{j})}\right)^2 \sum_{j=1}^{Q} \left(f_{tran.}^{(\mathrm{j})} - \overline{f}_{tran.}^{(\mathrm{j})}\right)^2}} \tag{3}$$

Where $f_{sim.}^{(\mathrm{j})}$ and $\overline{f}_{sim.}^{(\mathrm{j})}$ are the simulated neutron intensity on each pixel of PSF, and the averaged neutron intensity on PSF, respectively, when source is off the center; $f_{tran.}^{(\mathrm{j})}$ and $\overline{f}_{tran.}^{(\mathrm{j})}$ are the corresponding intensities obtained by translation of the PSF when the source at the center; $cc \in [0, 1]$. A smaller *CC* indicates higher degree of spatially translational variance. According to the correlation coefficients, the degree of spatially translational variance of PSFs for the four types of coded apertures is as follows: array hole > pin hole > IRC > cone hole. It is notable that the integrated neutron intensity is as follows: cone hole > array hole >> IRC hole ≈ Pin hole, which hints the linear characteristic of imaging system of cone hole may be destructed due to its large aperture size. In addition, *CC* can also be used to measure the reconstruction accuracy of reconstructed image, compared with source image. A larger *CC* indicates higher reconstruction accuracy.

3. Results and discussion

3.1. Image quality assessment

To quantitatively assess the reconstruction accuracy of reconstructed image, two indicators were applied. One is the correlation coefficient described by Eq. (3). The other is the peak to noise ratio (PSNR), which is expressed as:

$$PSNR = 10\log_{10}\left(\frac{MSE}{S^2}\right) \tag{4}$$

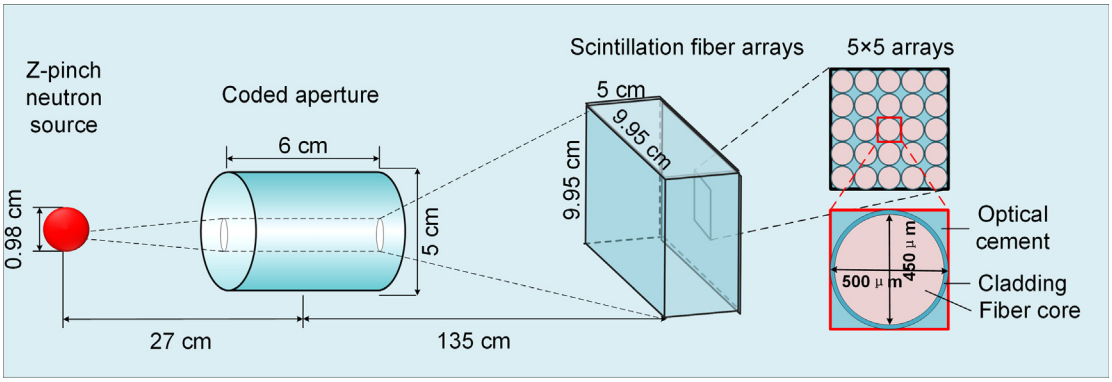

Fig. 4. Neutron coded imaging setup for diagnosis of Z-pinch driven fusion source.

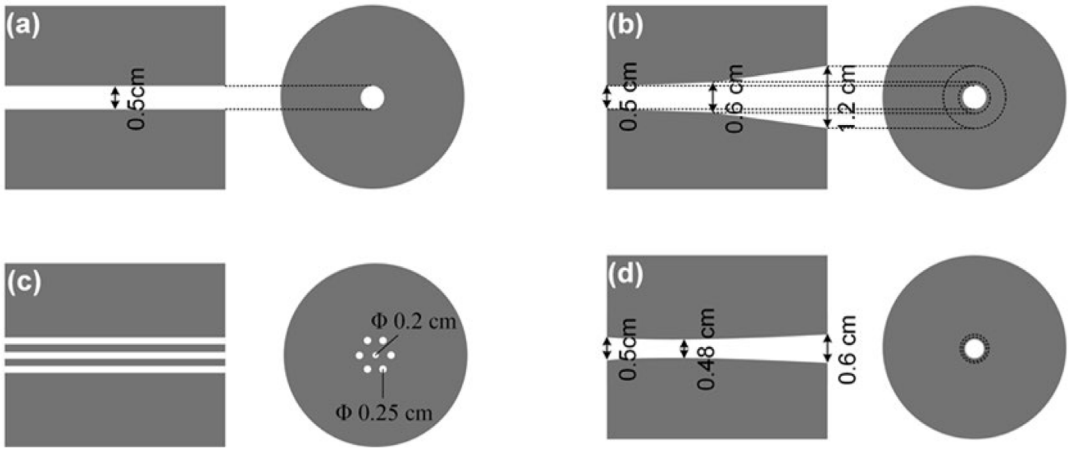

Fig. 5. Different types of coded apertures: (a) pin hole; (b) cone hole; (c) array hole; (d) IRC hole.

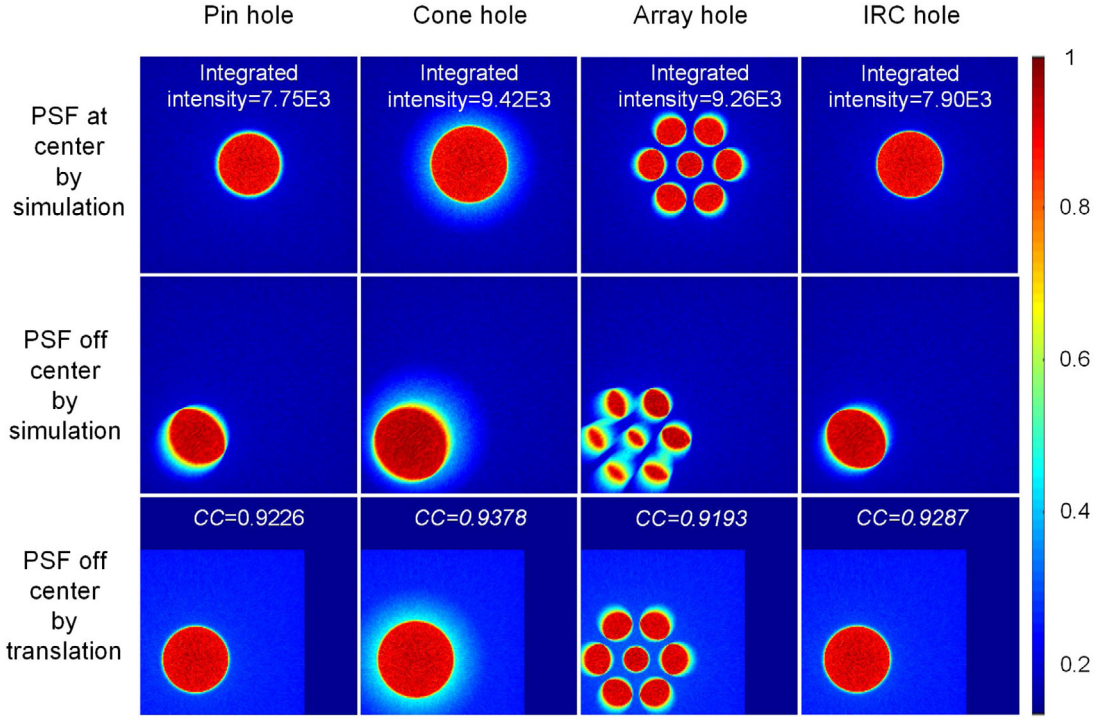

Fig. 6. Spatially translational variance of PSFs for different types of coded apertures.

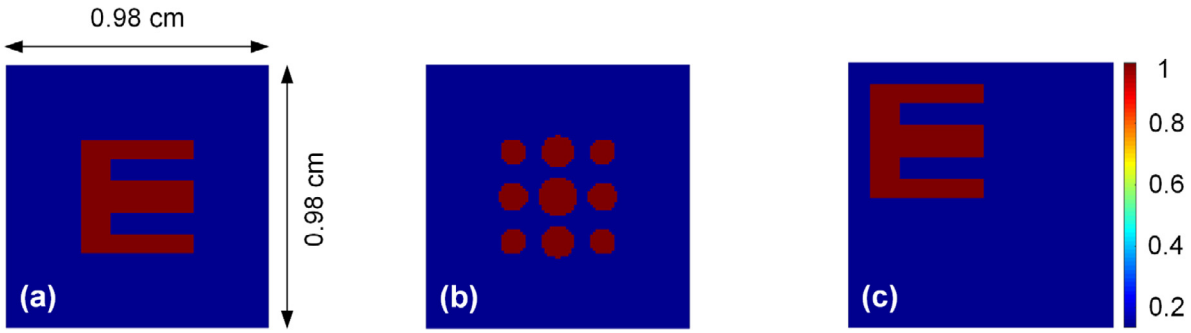

Fig. 7. Source images of three types of phantoms: (a) "E" letter; (b) "multiple bubbles" letter; (c) offset "E" letter.

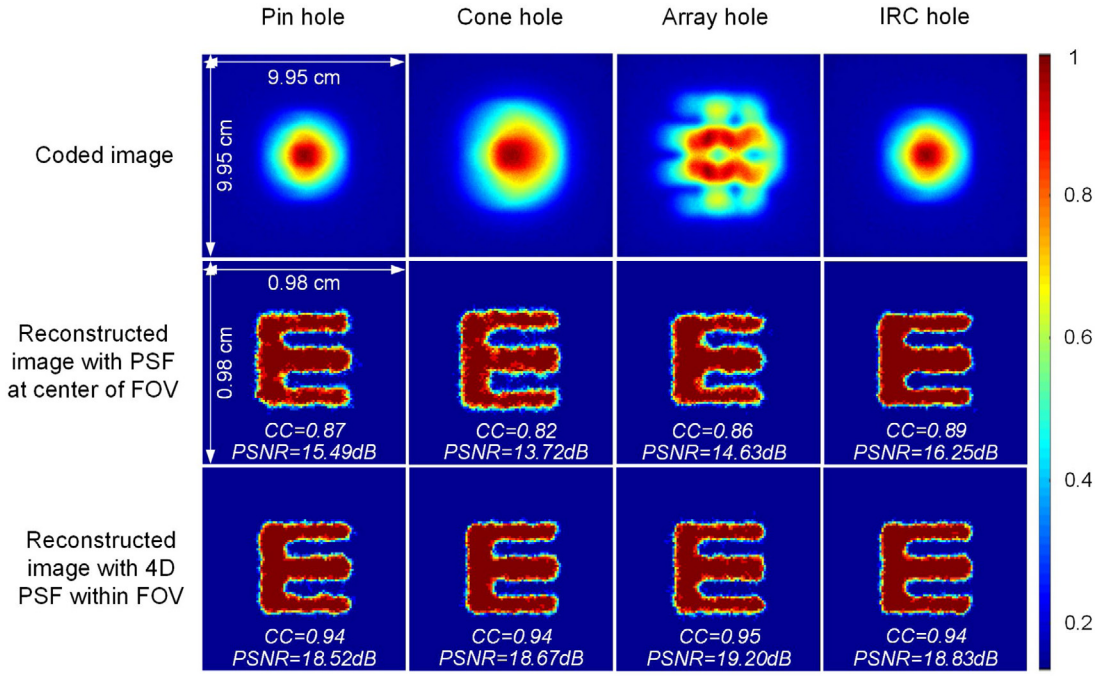

Fig. 8. Coded images and reconstructed source images of "E" letter at the center of FOV under different types of apertures.

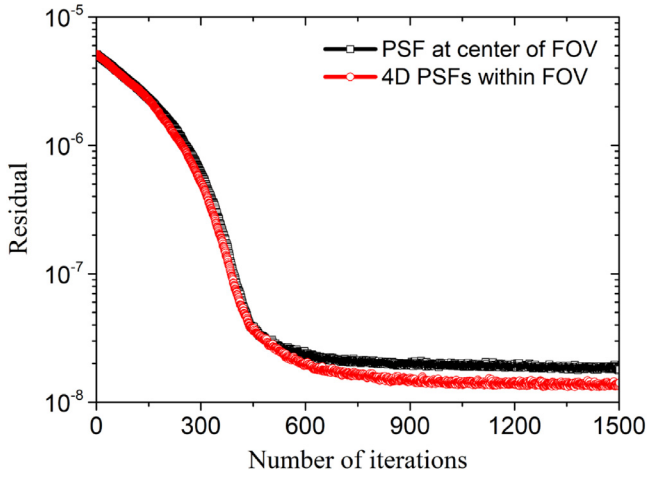

Fig. 9. Comparison of residuals of reconstructions for "E" letter with different types of PSF under pin hole.

Where S is the maximum pixel value in the image. MSE is the mean squared error between two images, which can be defined as:

$$MSE = \frac{1}{Q}\sum_{j=1}^{Q}\left(\hat{x}_j - x_j\right)^2 \tag{5}$$

Where $\hat{x}_j$ and x_j are the reshaped reconstructed image and source image, respectively. The unit of *PSNR* is dB. A larger *PSNR* indicates higher reconstruction accuracy.

3.2. Reconstructions for sources at the center of FOV

To show the performance of 4D PSFs on addressing the limitations of non-linear imaging system, spatially variant PSF, and system misalignment, we compared the reconstructions with PSFs at the center of FOV and with 4D PSFs under different types of coded apertures. As shown in Fig. 7, three types of phantoms, "E" letter, more complex "multiple bubbles" letter at the center of FOV, and "E" letter off the center of FOV by 0.49 cm horizontally and 0.49 cm vertically, were used as the source images to be reconstructed, which have a total size of 0.98 × 0.98 cm^2 and 0.429 × 0.429 cm^2 for the central letters, respectively. The size of each part varies in each letter, with the minimum width of 0.078 cm in the "E" letter, and the minimum

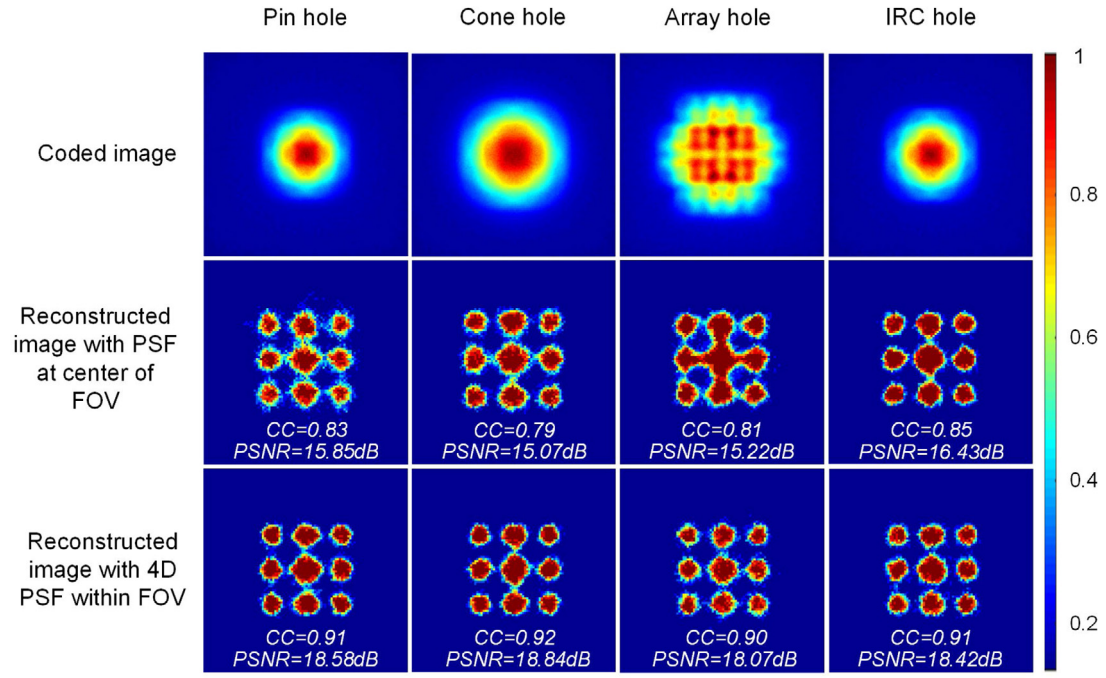

Fig. 10. Coded images and reconstructed source images of "multiple bubbles" letter at the center of FOV under different types of apertures.

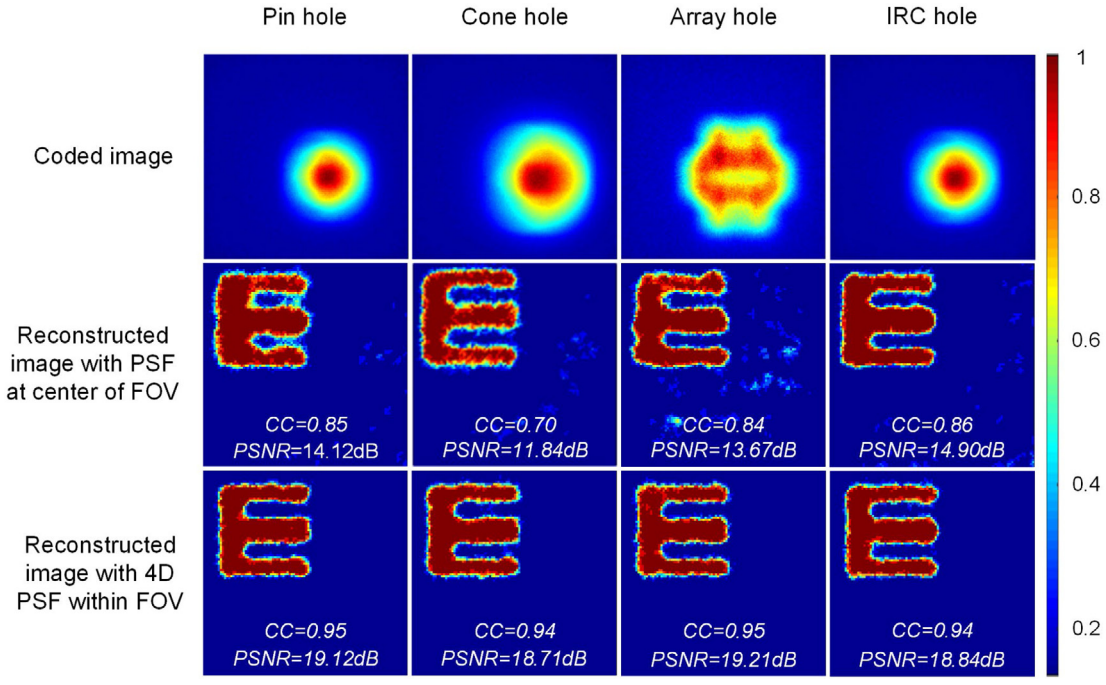

Fig. 11. Coded images and reconstructed source images of "E" letter off the center of FOV under different types of apertures.

diameter of 0.072 cm in the "multiple bubbles" letter. In the reconstruction, 2D convolution between the source image and the PSF was calculated as follows: (1) transforming the two images from spatial domain to frequency domain by Fourier transform, respectively; (2) multiplying the two images in frequency domain; and (3) transforming the multiplied result from frequency domain to spatial domain by inverse Fourier transform. To ensure fair comparisons of reconstructed images, we tried to make the IAGA algorithm show its best performance in each reconstruction by using the optimal parameters, which were selected according to the largest PSNR by sweeping out the parameter space, in particular the sparse coefficient α_{TV}.

Fig. 8 shows the simulated coded images and reconstructed images of "E" letter at the center with PSF at the center of FOV and with 4D PSFs, respectively. Notably, same as the cross section of scintillation fiber arrays, coded images have a size of 9.95×9.95 cm^2; same as the source image, reconstructed images have a size of 0.98×0.98 cm^2. In general, the code images are blurred by four types of coded apertures, but the "E" letter can be identified after image reconstruction. *CC* and *PSNR* of images reconstructed with PSF at the center of FOV are as follows: IRC hole > pin hole > array hole > cone hole. Because of good performance to treat spatially translational variance of PSF, IRC hole achieves the best result. As the cone hole has the largest aperture size, which may destruct the linear characteristic of imaging system, resulting in the worst result. However, *CC* and *PSNR* of images reconstructed with 4D PSFs under different types of coded apertures are similar but systematically larger, compared with reconstructions with PSF at the center of FOV. Its advantage can also be observed from smaller residual in the iterations, as shown in Fig. 9. It indicates that reconstructions with 4D PSFs could treat limitations of non-linear imaging system and spatially variant PSF.

From the reconstructed images of "E" letter, we may feel that the reconstruction accuracy is acceptable because structures of the source image can be clearly identified with the PSF at the center of FOV. However, as shown in Fig. 10, obvious aberrations were observed in reconstructed images of "multiple bubbles" letter with PSF at the center of FOV. The neighborhood "bubbles" almost can barely be distinguished under cone hole and array hole, whereas reconstructions with 4D PSFs show good performance. Therefore, 4D PSFs are quite useful in reconstructing complex sources.

3.3. Reconstructions for sources off the center of FOV

To imitate the system misalignment in real neutron coded imaging, we observed the reconstruction accuracy of source image by offsetting the "E" letter source. As shown in Fig. 11, shape aberrations for offset source become more severe than those for the sources at the center reconstructed with PSF at the center of FOV, in particular the upper part of "E" letter; furthermore, lots of artifacts appear in the marginal region of the source image. That is because the spatially translational variance of PSF becomes more severe as the off-center distance increases. However, almost the same reconstruction accuracy was observed in reconstructions with 4D PSFs. It clearly demonstrates that 4D PSFs is a powerful tool to address the problem of system misalignment.

4. Conclusions

We have presented the limitations of non-linear imaging system, spatially variant PSF, and system misalignment in neutron coded imaging under current reconstruction scheme. Image reconstructions with 4D PSFs were proposed to address those limitations. Comparative study of reconstructions for different complexities of phantoms at and off the center with the PSF at the center of FOV and with 4D PSFs was performed. The results demonstrate reconstructions with 4D PSFs always achieve a similar reconstruction accuracy no matter with the type and size of coded apertures, as well as precision of system alignment, whereas those with the PSF at the center of FOV show a different but systematically lower reconstruction accuracy. Reconstructions with 4D PSFs can significantly lighten the burden of coded aperture design and system alignment in neutron coded imaging.

Notably, 4D PSFs used in current reconstruction is calculated from Monte Carlo simulation. The method to obtain the real one in experiment will be further investigated in the future.

CRediT authorship contribution statement

Mingfei Yan: Methodology, Software, Writing – original draft. **Huasi Hu:** Supervision, Conceptualization. **Guang Hu:** Investigation, Formal analysis. **Yihong Yan:** Data curation, Visualization. **Zhihua Liu:** Validation, Writing – review & editing.

Declaration of competing interest

The authors declare that they have no known competing financial interests or personal relationships that could have appeared to influence the work reported in this paper.

Acknowledgments

This research is supported by the NSAF Joint Fund of China (Grant No. U1830128) and the National Natural Science Foundation of China (Grant No. 11975182).

References

[1] E.E. Fenimore, T.M. Cannon, Coded aperture imaging with uniformly redundant arrays, Appl. Opt. 17 (1978) 337–347.
[2] D. Ress, R.A. Lerche, R.J. Ellis, S.M. Lane, K.A. Nugent, Neutron imaging of laser fusion targets, Science 241 (1988) 956–958.
[3] I. Thfoin, O. Landoas, T. Caillaud, L. Disdier, J.L. Bourgade, B. Rossé, T.C. Sangste, V.Y. Glebov, High resolution neutron imaging for inertial confinement fusion experiments, in: 1st International Conference on Advancements in Nuclear Instrumentation, Measurement Methods and their Applications, IEEE, 2010.
[4] C. Lynde, F. Carrel, V. Schoepff, C. Frangville, R. Woo, A. Sardet, J. Venara, M.B. Mosbah, R.A. Khalil, Z.E. Bitar, Demonstration of coded-aperture fast-neutron imaging based on timepix detector, Nucl. Instrum. Methods Phys. Res. Sect. A 954 (2020) 161373.
[5] P. Bingham, H. Santos-Villalobos, K. Tobin, Coded source neutron imaging, Proc. SPIE-IS & T 7877 (2011) 78770M.
[6] S. Wang, Y.B. Zou, X.S. Zhang, Y.R. Lu, Z.Y. Guo, Coded source imaging simulation with visible light, Nucl. Instrum. Methods Phys. Res. Sect. A 651 (2011) 187–191.
[7] M.F. Yan, H.S. Hu, G. Hu, Z.H. Liu, C. He, Q. Yi, Comparison of heuristic and deterministic algorithms in neutron coded imaging reconstruction, Nucl. Instrum. Methods Phys. Res. Sect. A 985 (2021) 164704.
[8] W.H. Richardson, BayesIan-based iterative method of image restoration, J. Opt. Soc. Amer. 62 (1972) 55–59.
[9] M.C. Ghilea, T.C. Sangster, D.D. Meyerhofer, Aperture tolerances for neutron-imaging systems in inertial confinement fusion, Rev. Sci. Instrum. 79 (2008) 023501.
[10] M.J. Cieslak, K.A.A. Gamage, R. Glover, Coded-aperture imaging systems: past, present and future development - A review, Radiat. Meas. 92 (2016) 59–71.
[11] M.J. Gieles, H.W.A.M. Jong, F.J. Beekman, Monte Carlo simulations of pinhole imaging accelerated by kernel-based forced detection, Phys. Med. Biol. 47 (2002) 1853–1867.
[12] K.A. Nugent, B. Luther-Davies, Application of penumbral imaging to thermonuclear neutrons, J. Appl. Phys. 58 (1985) 2508–2515.
[13] L. Disdier, A. Rouyer, D.C. Wilson, A. Fedotoff, C. Stoeckl, J.-L. Bourgade, V.Y. Glebov, J.-P. Garconnet, W. Seka, High-resolution neutron imaging of laser imploded DT targets, Nucl. Instrum. Methods Phys. Res. Sect. A 489 (2002) 496–502.
[14] T. Ueda, S. Fujioka, S. Nozaki, R. Azuma, Y.-W. Chen, H. Nishimura, A uniformly redundant imaging array of penumbral apertures coupled with a heuristic reconstruction for hard X-ray and neutron imaging, Rev. Sci. Instrum. 81 (2010) 073505.
[15] P. Volegov, C.R. Danly, D.N. Fittinghoff, G.P. Grim, N. Guler, N. Izumi, T. Ma, F.E. Merrill, A.L. Warrick, C.H. Wilde, D.C. Wilson, Neutron source reconstruction from pinhole imaging at national ignition facility, Rev. Sci. Instrum. 85 (2014) 023508.
[16] A.L. Velikovich, R.W. Clark, J. Davis, Y.K. Chong, C. Deeney, C.A. Coverdale, C.L. Ruiz, G.W. Cooper, A.J. Nelson, J. Franklin, L.I. Rudakov, Z-pinch plasma neutron sources, Phys. Plasmas 14 (2007) 022701.
[17] G.E. Sommargren, R.A. Lerche, Collimator design for neutron imaging of laser-fusion targets (UCID—19317), 1981, United States.
[18] D. Ress, Design of thick apertures for high-resolution neutron penumbral imaging, IEEE Trans. Nucl. Sci. 37 (1990) 155–160.
[19] I. Thfoin, O. Landoas, T. Caillaud, L. Disdier, M. Vincent, J.-L. Bourgade, B. Rossé, T.C. Sangster, V. Yu. Glebov, G. Pien, W. Armstrong, Alignment effects on a neutron imaging system using coded apertures, Rev. Sci. Instrum. 81 (2010) 033503.
[20] E.J. Candès, J. Romberg, T. Tao, Robust uncertainty principles: exact signal reconstruction from highly incomplete frequency information, IEEE Trans. Inform. Theory 52 (2006) 489–509.
[21] MCNP6 users Manual - Code Version 6.1.1beta, 2014, LA-CP-14-00745.